

Finite element based prediction of process-induced deformation of autoclaved composite structures using 2D process analysis and 3D structural analysis

G. Fernlund^{a,*}, A. Osooly^a, A. Poursartip^a, R. Vaziri^a, R. Courdji^a, K. Nelson^b,
P. George^b, L. Hendrickson^c, J. Griffith^d

^a *Departments of Metals and Materials Engineering and Civil Engineering, The University of British Columbia, 309-6350 Stores Road, Vancouver, BC, V6T 1Z4, Canada*

^b *Boeing Phantom Works, P.O. Box 3999 MC 73-09, Seattle, WA 98124-2499, USA*

^c *Boeing Canada Technology, 99 Murray Park Road, Winnipeg, Manitoba R3J 3M6, Canada*

^d *Boeing Advanced Manufacturing Technologies, St. Louis, USA*

Abstract

Dimensional control of composite components is critical for cost effective manufacturing of large composite aerospace structures. This paper presents an engineering approach to the prediction of process-induced deformations of three-dimensional (3D) autoclaved composite components. A 6-step method that uses a two-dimensional (2D) special purpose finite element (FE) based process simulation code and a standard 3D structural FE code is presented. The approach avoids the need to develop a full 3D process model, significantly reducing the computational effort yet retaining much of the detail required for accurate analysis. The methodology is presented together with numerical examples and two case studies demonstrating the validity, utility, and limitations of the approach.

© 2003 Elsevier Ltd. All rights reserved.

Keywords: Composite structures; Process-induced deformations; Finite element analysis; Dimensional control; Process modelling

1. Introduction

Process-induced deformations affect dimensional control of autoclaved processed parts. Poor dimensional control leads to increased cost in assembly, or in critical cases, the need to scrap parts. There are a number of ways to address the problem of process-induced deformations (Fig. 1). For example, it can be addressed in the design of a part by avoiding curved structures, bonding joints at room temperature, and using fasteners for assembly. These are very conservative approaches that do not give cost effective unitized structures. Process-induced deformations can also be addressed in assembly by the use of hard or mouldable shims to fill gaps between mating structures. This approach requires that there is clearance between mating parts, and is typically achieved by designing in gaps between mating parts. Another approach is mould geometry compensation,

where the tool is compensated to counteract process-induced deformations. Two issues with this approach is that the deformation must be known before the tool is made, and that process-induced deformations often vary slightly from part-to-part. Nevertheless, using this approach, the number of shims used can be reduced, if not completely eliminated, and significant cost savings achieved. Mould geometry compensation, and specifically the prediction of the process-induced deformations to obtain mould compensation factors, is the focus of this paper.

Process-induced deformations of autoclaved composite structures are the result of stress acting on, or stress generated within, the structure during processing. The stress acting on the structure typically arises from the autoclave pressure applied on the bag side and differential expansion of the tool and part on the tool side [1,2] (Fig. 2). The main effect of the autoclave pressure is observed early in the cure cycle where it leads to resin flow and thickness changes in the part. In systems where resin is bled off on the bag side, autoclave pressure can cause gradients in the fibre volume fraction, which leads

* Corresponding author. Tel.: +1-604-822-3673; fax: +1-604-822-3619.

E-mail address: goran.fernlund@ubc.ca (G. Fernlund).

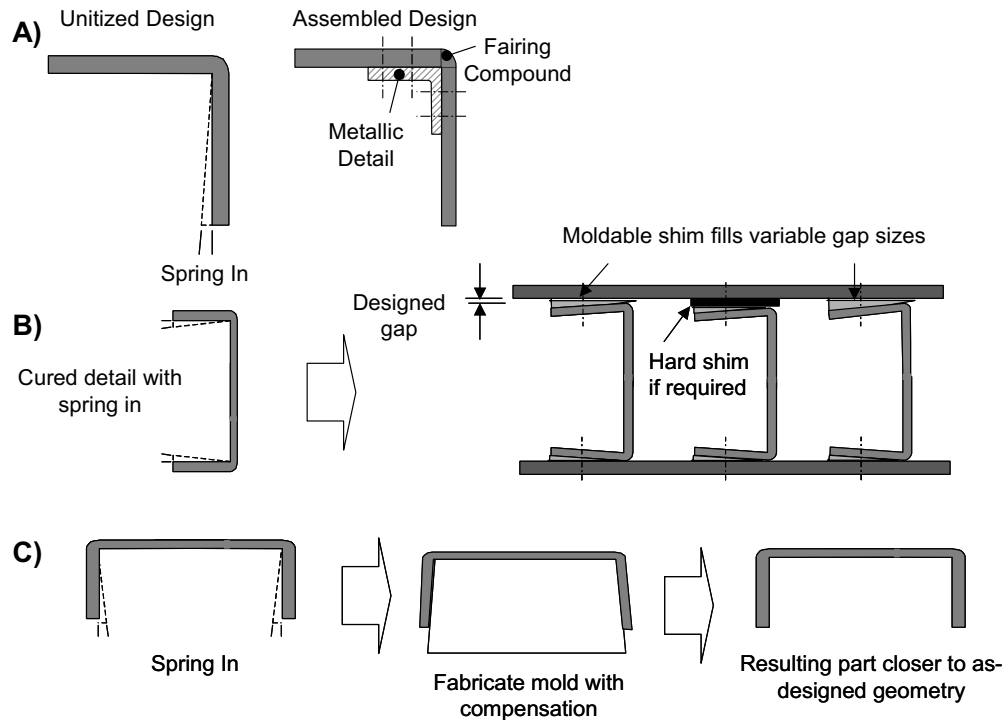


Fig. 1. Different ways to address process-induced deformations: (A) design compensation; (B) assembly compensation; (C) mould geometry compensation.

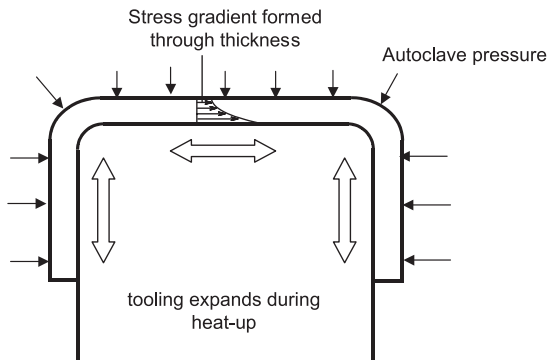


Fig. 2. Stress acting on a composite laminate during processing. On the bag-side, autoclave pressure, and on the tool-side, tool-part shear stress.

to warpage of the structure [1,3]. An indirect effect of the autoclave pressure is that it increases the amount of stress transferred to the part on the tool side, a phenomena often called tool-part interaction. This interaction often causes a residual in-plane stress gradient through the thickness of the part, which results in warpage when the part is removed from the process tool [1,2]. Residual stress is also developed due to internal volume changes where the main drivers are anisotropic thermal expansion and resin cure shrinkage, which cause micro- and macro-mechanical stress build-up in the corners of curved laminates leading to spring-in or spring-forward [3–6].

There are two levels of residual stress in a fibre-reinforced polymer: micro-mechanical, acting on the fibre matrix level; and macro-mechanical, acting on the ply and laminate levels. Micro-mechanical residual stresses affect the strength of the structure but not process-induced deformations, and averages out at the level of a ply or higher. It is the gradients in residual macro-mechanical stresses through the thickness of the laminate that are the main cause of process-induced deformations. Note that if the structure can deform to relieve the residual stress, which often is the case when a thin-walled structure is removed from the process tooling, the structure is essentially stress free on the macro-mechanical level.

This paper addresses how process-induced deformations of composite parts can be predicted and mould compensation factors obtained using finite element analysis. The paper specifically looks at how two-dimensional (2D) process models can be used together with three-dimensional (3D) structural models to predict deformations of complex 3D geometries using a combined 2D/3D modelling technique. The paper begins with a brief description of 2D process models followed by a simple case study illustrating the basic concepts of the developed 2D/3D technique. The technique is formalized into a six-step procedure and the limitations and range of applicability is discussed and illustrated with numerical examples. The technique is then applied to a complex aerospace structure where predicted and measured process-induced deformations are compared.

2. 2D process models

There are simple formulas in the literature based on geometric arguments that in special cases do a good job of predicting spring-in of curved composite structures [5,6]. However, to accurately simulate general process-induced deformations of a composite structure, a more comprehensive process model is needed. The factors that drive deformations can be classified as intrinsic, or material related, and extrinsic, or part and process related. Examples of intrinsic factors are anisotropic thermal expansion and resin cure shrinkage, and examples of extrinsic factors are lay-up, part and tool geometry, cure cycle, tool material, tool surface, and caul-sheets. There have been several analytical and numerical process models developed that predict residual stress build-up and process-induced deformations of composite structures, e.g. [7–15]. These models differ mainly in the number of factors that are accounted for, the phenomena simulated, and the complexity of the constitutive models used. A model that was specifically designed to account for the previously mentioned intrinsic and extrinsic process parameters is COMPRO [16–20]. This model determines component internal temperature, resin degree of cure, resin flow and the development of residual stress and deformation. The model advances previous work in a number of ways, allowing modelling of complex 2-D structures with multiple composite and non-composite materials, including the effects of process tooling. A ‘virtual

autoclave’ simulation is used to predict the boundary conditions to which parts are actually subjected during processing. Although increased complexity and detail in process models typically lead to more accurate predictions, the more detailed and complex the model is, the more time consuming it is to set-up, run, and analyze the results. The most useful model from an engineering point-of-view is one with the right balance between detail, rigour and simplifying assumptions.

3. 2D/3D technique

A 2D/3D technique based on a 2D process model and a 3D structural model will be introduced with a case study where measured and predicted process-induced deformations of a composite rib are compared.

3.1. Case study I: the T-45 rib

The T-45 rib is a ‘box’ structure with one side open that consists of eight layers of AS4/977-3 woven carbon/epoxy prepreg $[0/45_3]_s$, and is processed on a convex aluminum tool [21]. Fig. 3A shows a schematic top view of the initial and deformed shape of the rib, Fig. 3B shows a top and bottom view of two manufactured ribs, and Fig. 3C shows how process induced deformations were measured using an hand caliper. Five manufactured ribs were measured for process-induced deformations. Measurements showed that the main deformation

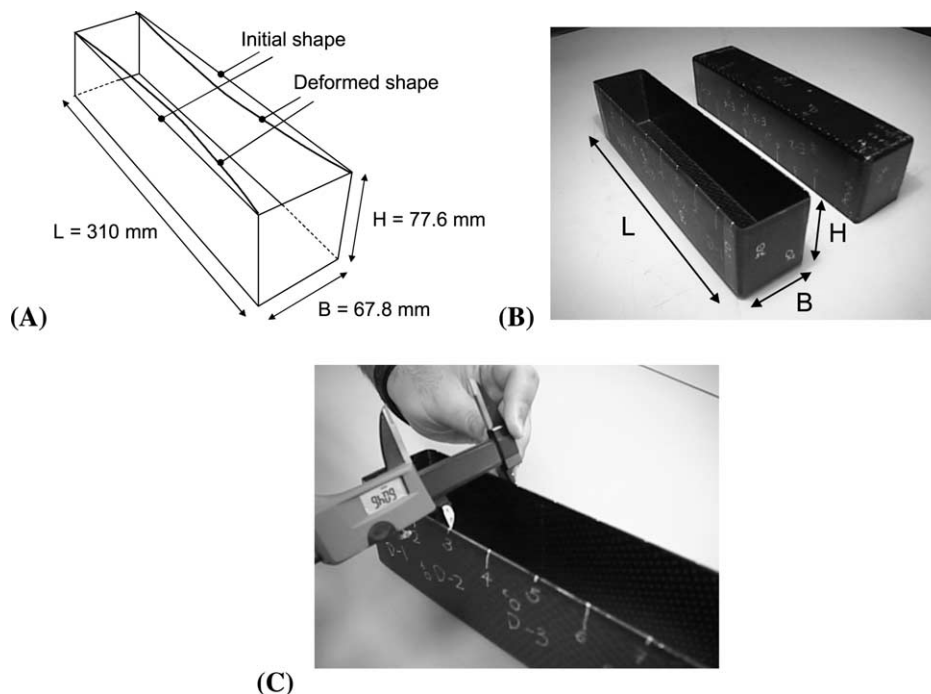


Fig. 3. (A) Schematic top view of the T-45 rib showing initial and deformed shape; (B) top and bottom view of manufactured rib; (C) measurement of flange-to-flange distance (spring-in) on intact rib.

of the ribs was flange spring-in along the length of the ribs (Fig. 3A). To quantify this, the flange-to-flange distance was measured at the inner mould surface of the part with a digital hand caliper (Fig. 3C), and the flange spring-in angle was calculated along the length of the rib. The rib was then cut into sections and the flange-to-flange distance was re-measured on the sectioned rib (Fig. 4).

Fig. 5 shows the measured spring-in angle, θ , before and after sectioning of the five ribs, denoted part A to part E. The figure clearly shows that the flange spring-in varies along the length of the ribs before sectioning and is approximately constant for the sectioned ribs, although there is variability in magnitude between the five ribs. The spring-in of the sectioned rib sections is in the following referred to as free spring-in, the spring-in of a section when it is not constrained by the surrounding structure. Fig. 5 shows that the difference between the free and constrained spring-in is largest at the ends of the ribs, where the flanges are prevented from springing in. These measurements indicate that the rib sections act independently during processing and that all interactions

between sections are geometrical, and occur when the rib is fully cured and removed from the tool.

To predict the process-induced deformations of the ribs, a 2D plane strain finite element (FE) model of a rib cross-section was first created in COMPRO (version 2.41) to calculate the free flange spring-in. As the cross-section is symmetric, only half of the section was modeled (Fig. 6). The centre of the solid tool is hollowed out in the FE mesh to simplify the meshing and to reduce the degrees of freedom of the model. The effect of mesh density on the predicted results was not examined in the present study but the used mesh density was based on previously performed convergence studies with similar geometries. Convective heat transfer was applied to all boundaries exposed to the autoclave gas, i.e., along the outer perimeter of the part, and along the lower horizontal tool surface. All other outer boundaries were set to adiabatic. The vacuum bag and breather were not explicitly modeled but their thermal effect is incorporated in an effective heat transfer coefficient, h , which is pressure dependent [18]. The effective heat transfer coefficient used was $h = 17 + P * 4.13 \times 10^{-5}$ [W/m²K],

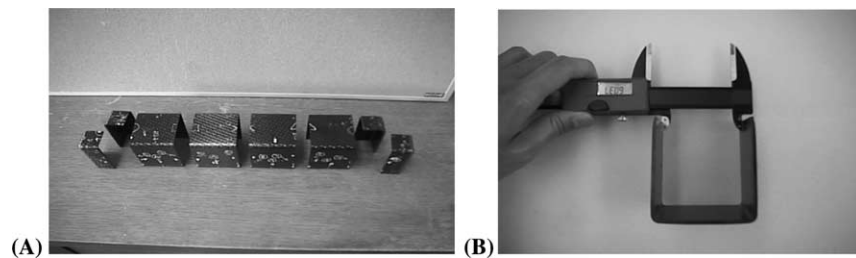


Fig. 4. (A) Sectioned rib; (B) spring-in measurements on sectioned rib.

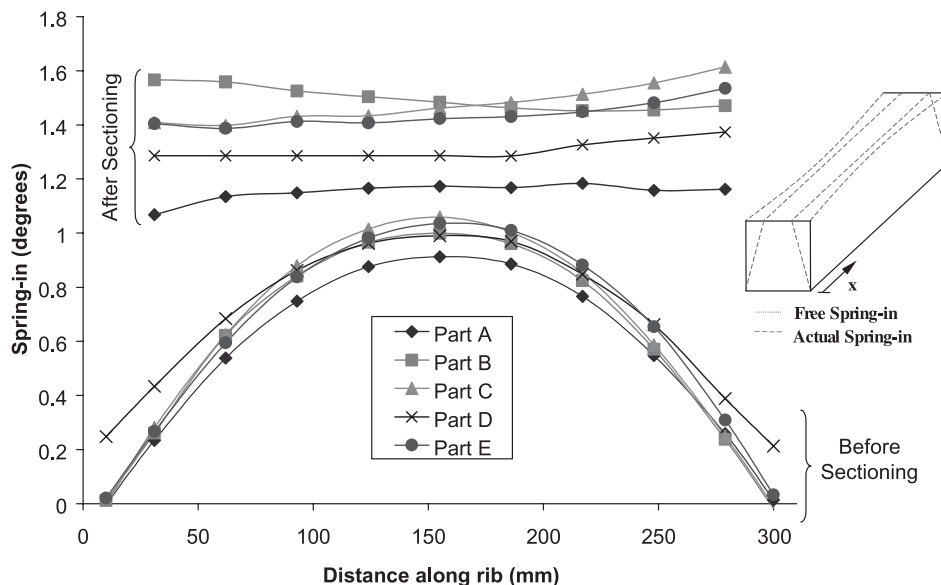


Fig. 5. Measured spring-in angle, θ , before and after sectioning for five nominally identical ribs.

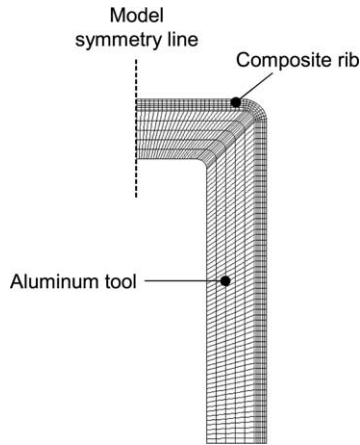


Fig. 6. FE model of half of a rib section including the aluminum process tool.

where P is the pressure in Pa. Autoclave pressure was applied to all boundaries exposed to convective heat transfer. Along the symmetry line on the web, the displacement condition was set to “sliding” so that tool and laminate could move freely in the vertical direction along this boundary. Finally, the point at the intersection of the symmetry line and the inner contour of the tool was set to “fixed”, i.e., no displacement in any direction, to prevent rigid body movement. The interface between the tool and laminate was “bonded”, and therefore no slip was allowed to occur.

COMPRO uses degree of cure of the resin and temperature as state variables that uniquely determine the thermo-physical properties of the composite laminate at any instant of the process [17,18]. Temperature is obtained from a heat transfer analysis and degree of cure is calculated based on the cure kinetics and the time-temperature history of the resin. Empirical cure rate equations for the composite material are determined based on DSC test for a range of constant temperatures and temperature ramp rates. The evolution of stiffness of the material is determined using fixed frequency DMA tests for different cure cycles, and master equations expressing the modulus development as a function of degree of cure and temperature are developed. For details of typical procedures and determination of other relevant properties, see [17,18]. The thermo-elastic material properties for the aluminum tooling were taken from the literature [24], see Table 1. Since there was no materials database available for the cure kinetics, modulus development, cure shrinkage, and thermal expansion for the AS4/977-3 material, properties of a similar prepreg system, Hexcel Style 3K-70-PW F593, were used in the model. The model predicted a free flange spring-in of 1.6° , about 15% higher than the average measured value of 1.4° .

To test and validate the 2D/3D technique for the ribs, the following approach was taken (Fig. 7): A 3D FE

Table 1
Material properties for aluminum tool [24]

Material property	Aluminum tooling
Density [kg/m^3]	2700
Specific heat [J/kgK]	896
Linear coefficient of thermal expansion [$10^{-6}/^\circ\text{C}$]	23.6
Thermal conductivity [W/mK]	167
Modulus of elasticity [GPa]	69

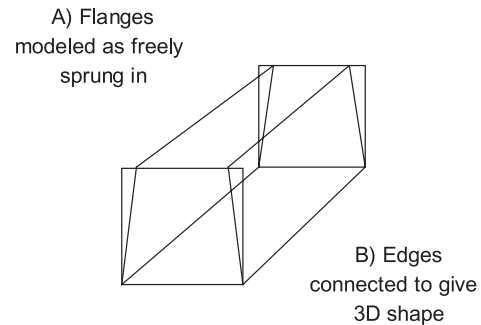


Fig. 7. Schematic of 3D shell model.

model of the rib was created in the commercial FEM code ANSYS (version 5.3) using orthotropic shell elements. The rib was modeled with its flanges uniformly sprung in, with the same spring-in as the average measured on the sectioned ribs, i.e. 1.4° (see Fig. 5). Since the measured and predicted free spring-in were close but not identical due to the lack of accurate material properties needed for the process model, the measured spring-in was used in the analysis instead. At this stage the structure is stress free and the vertical edges of the rib do not match up (Fig. 7). The ends of the long flanges were then displaced to match up with the edges of the ends of the rib. The 3D rib was modeled as an elastic fully cured composite. With all edges connected, the FE program (ANSYS) calculated the 3D shape of the rib. Again, because the properties of the AS4/977-3 material were not known at the time of modelling, the properties of the fully cured Hexcel Style 3K-70-PW F593, was used in the 3D shell model.

Fig. 8 shows a comparison between predicted and average measured spring-in. Overall the predictions are in very good agreement with the measurements. The shape of the spring-in angle vs. distance along rib profile is predicted correctly and the magnitude is off by less than 0.1° .

3.2. Six-step methodology

Case study I showed that during processing, there is little or no interaction between different cross-sections of the 3D structure because the component cannot deform away from the stiff tool during processing. This means

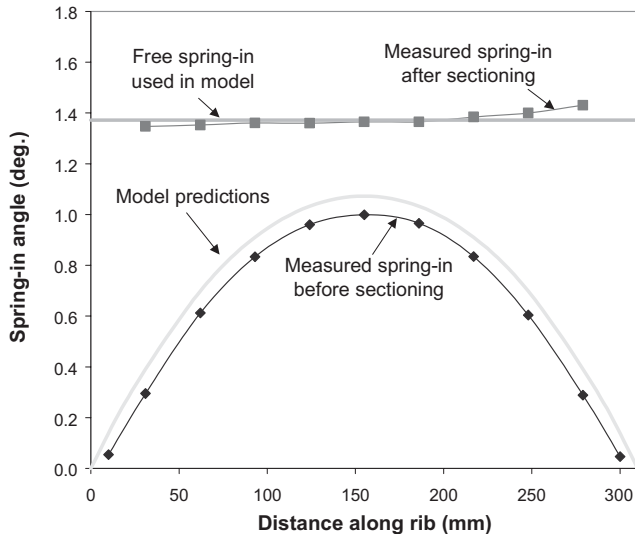


Fig. 8. Comparison of average measured and predicted flange spring-in. Measure values are the average of five different ribs.

that a 2D process model can be used to determine the “free” deformations of various cross-sections and the geometrical interaction can be addressed in a simple elastic 3D model when the part is fully cured. In case study I, the geometry was relatively simple, but the technique can be formalized into a more general six-step methodology.

Step 1. Select appropriate 2D sections of the 3D structure. This step requires some engineering judgment but the following guidelines can be given. Select 2D sections where the out-of-plane deformations are expected to be large, i.e., where the residual stresses are expected to be large and/or where the cross-sectional stiffness is low. If the cross-sectional geometry or material properties are non-uniform, use more than one cross-section. The larger the number of cross-sections, the more accurate the result will be. In case study I, only one cross-section perpendicular to the length of the rib was used because of the uniformity of the part. A cross-section perpendicular to the short flange was not used because of the large resistance of the flanges to deformation in this plane (Fig. 3).

Step 2. Create and run 2D process models of the selected sections. Create 2D process models of the selected cross-sections using an appropriate process model that accurately simulates residual stress build-up and deformations.

Step 3. Study and verify the predicted deformations of the 2D models. Verify that the model predictions agree with measured or expected results qualitatively and quantitatively to ensure fidelity of the model.

Step 4. Create a 3D model of the part. Create a simple elastic shell (or similar) model of the fully cured part and use the material properties of the fully cured composite materials. Although 2D process models in general re-

quire a high mesh density, a low mesh density shell model is often sufficient for this 3D interaction analysis.

Step 5. Isolate cross-sections in the 3D model and match deformations. In this step the mechanical loads that need to be applied to the 3D structure to match the predicted deformations of the 2D process models are determined. Create unit width shell models (plane-strain beam models) corresponding to the 2D sections modeled in the 2D process model. Thickness and modulus of elasticity at each corresponding point should be the same for both the unit width shell model and the 2D process model. To match deformations between the 2D process model and the unit width shell model, some engineering judgment is required. The objective is to find one or more moments per unit length to be applied to the unit width shell model that give the same deformations as the 2D process model. The rationale for using moments is that the important deformation of most shell structures is out of plane, caused by through-thickness gradients of residual in-plane stresses. In-plane deformations are typically too small to be of practical significance.

The following guidelines should be observed in this step. Moments should be applied at locations where the part has the greatest change of curvature due to residual stress. The number of applied moments and chosen deformations should be the same, but their location can be different. As the number of applied moments increases, the deviation between the deformed shape of the process model and unit width shell model will decrease. The deformations chosen for matching purposes can be rotations or displacements and important deformations from a manufacturing point-of-view should be selected. The magnitude of the applied moments can readily be determined using the principle of superposition, as illustrated in case study II below.

Step 6. 3D-interaction analysis. A simple elastic 3D shell model of the composite component is created in a general-purpose FE code. The tool or other process conditions are not included and the element size can typically be fairly large. The moments calculated in the previous step are typically applied as line moments, varying linearly between parallel cross-sections, if applicable. The methodology is illustrated in case study II. However, before presenting case study II, the accuracy and range of applicability of the technique will be assessed.

3.3. Accuracy and range of applicability of the 2D/3D technique

To examine the accuracy and range of applicability of the proposed 2D/3D technique, consider a flat composite laminate as that in Fig. 9. According to classical lamination theory, e.g. [23], the stresses in the laminate can be expressed in terms of the resulting forces and

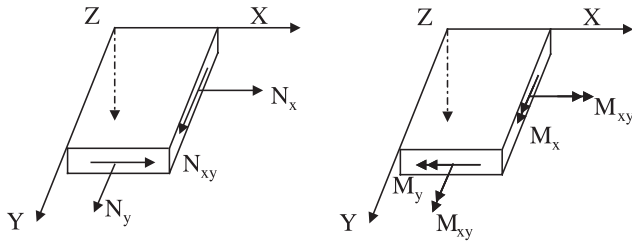


Fig. 9. Flat composite laminate with forces and moments applied.

moments per unit length, and the deformations in terms of mid-plane strains and curvatures. The mid-plane strains, ϵ^0 , and curvatures, κ , are related to the in-plane forces, \mathbf{N} , and the moments, \mathbf{M} , through the A' B' D' compliance matrix (see Eq. (1)).

$$\begin{Bmatrix} \epsilon_x^0 \\ \epsilon_y^0 \\ \gamma_{xy}^0 \\ \kappa_x \\ \kappa_y \\ \kappa_{xy} \end{Bmatrix} = \begin{bmatrix} A'_{11} & A'_{12} & A'_{16} & B'_{11} & B'_{12} & B'_{16} \\ A'_{12} & A'_{22} & A'_{26} & B'_{12} & B'_{22} & B'_{26} \\ A'_{16} & A'_{26} & A'_{66} & B'_{16} & B'_{26} & B'_{66} \\ B'_{11} & B'_{12} & B'_{16} & D'_{11} & D'_{12} & D'_{16} \\ B'_{12} & B'_{22} & B'_{26} & D'_{12} & D'_{22} & D'_{26} \\ B'_{16} & B'_{26} & B'_{66} & D'_{16} & D'_{26} & D'_{66} \end{bmatrix} \begin{Bmatrix} N_x \\ N_y \\ N_{xy} \\ M_x \\ M_y \\ M_{xy} \end{Bmatrix} \quad (1)$$

A study of how well the 2D/3D approach works for flat laminates with different lay-ups will now be presented. As we do not have a 3D process model to compare against, we cannot in general determine the accuracy of the 2D/3D approach for plate and shell structures. However, in the following study we will use thermal loads on a fully cured laminate to simulate process-induced deformations of the 3D structure. The validation study proceeds as follows (Fig. 10):

- (A) Isolate two perpendicular strips of the laminate, one in the x -direction and one in the y -direction.
- (B) Create FE models of the two strips (plane strain beam models) and apply a defined thermal through-thickness gradient to the strips. Record the out-of-plane displacement, and determine the magnitude of the mechanical moment, applied to the ends of the strip, that gives the same deformation as the thermal gradient. This is straightforward, see case study II. Follow the above procedure for the strips in both the x - and the y -directions.

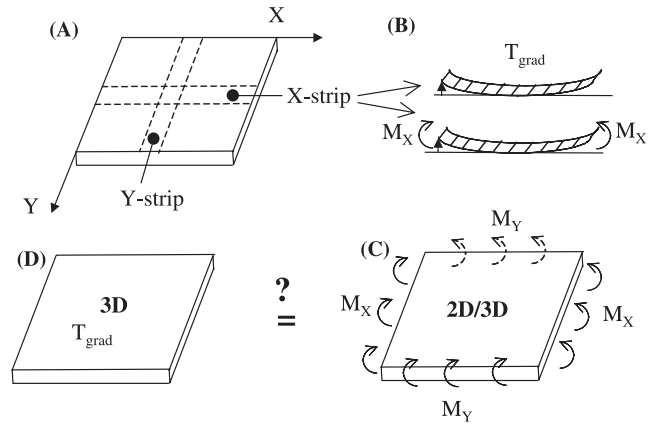


Fig. 10. Schematic of validation study.

- (C) Apply the moments determined in (B) along the edges of a finite element model of the entire laminate and record the deformations.
- (D) Apply the defined thermal gradient to the FE model of the entire laminate and record the out-of-plane displacements. Compare the deformations from (C) (2D/3D) and (D) (3D) to determine the accuracy of the 2D/3D method.

All laminates used in the validation study were square and had the dimensions $100 \times 100 \times 2$ mm (length, width, thickness), and all beam models had the dimensions $50 \times 5 \times 2$ mm (length, width, thickness). Only half the plate was modeled due to symmetry. Laminates made of graphite/epoxy consisted of sixteen plies with an individual ply thickness of 0.125 mm. The applied temperature gradient varied linearly through the thickness of the laminates, with a temperature of 0°C at the center and a temperature of $+50^\circ\text{C}$ and -50°C at the top and bottom faces, respectively. Table 2 shows the material properties used in the validation study.

The validation study was performed using the FE code ABAQUS (version 5.8). The analysis was a one-step static analysis and 4-noded composite shell elements were used for both plate and beam models. To simulate plane strain beam or cylindrical bending conditions using shell elements of finite width, the following deformation constraints were imposed. For a beam model in the x -direction: $\epsilon_y = 0$, $\kappa_y = 0$, and $\kappa_{xy} = 0$, and for a beam model in the y -direction: $\epsilon_x = 0$, $\kappa_x = 0$, and $\kappa_{xy} = 0$, see Eq. (1).

Table 2
Material properties for the materials used in the validation study

Material	E_1 (GPa)	E_2 (GPa)	G_{12} (GPa)	ν_{12}	CTE_1 ($\mu^\circ\text{C}$)	CTE_2 ($\mu^\circ\text{C}$)
Aluminum	69	69	26.54	0.3	23	23
Steel	207	207	79.62	0.3	11.7	11.7
Graphite/epoxy	181	10.3	7.17	0.28	0.02	22.5

Table 3

Comparison of the relative difference in predicted deformations between the 3D and the 2D/3D approach

Laminate #	Lay-up	Relative difference between 3D and 2D/3D approach (%)	Bending-twisting coupling D'_{16}/D'_{66} (%)	Bending-twisting coupling D'_{26}/D'_{66} (%)
1	Al	0.0	0	0
2	Al/St	0.0	0	0
3	[0 ₈ /90 ₈]	0.8	0	0
4	Al($\nu = 0$)	0.0	0	0
5	Al/St ($\nu = 0$)	0.0	0	0
6	[0 ₈ /90 ₈]($\nu = 0$)	0.0	0	0
7	[45/−45] _{4S}	7.5	8.1	8.1
8	[45 ₂ /−45 ₂] _{2S}	15.4	16.2	16.2
9	[45 ₄ /−45 ₄] _S	34.0	32.5	32.5
10	[0/45/−45/90] _{2S}	6.7	2.6	6.5
11	[0 ₂ /45 ₂ /45 ₂ /90 ₂] _S	19.4	2.8	23.6
12	[45/−45] _{8T}	0.1	0	0
13	[45 ₂ /−45 ₂] _{4T}	0.3	0	0
14	[45 ₄ /−45 ₄] _{2T}	1.0	0	0
15	[45 ₈ /−45 ₈] _T	2.6	0	0

Table 3 shows a comparison of the predicted deformations using the 2D/3D and the 3D approach for some different laminates. Included in the table are the bending-twisting coupling influence factors D'_{12}/D'_{66} and D'_{26}/D'_{66} , which will be explained shortly. The table shows that the difference between the 3D and 2D/3D approaches is less than 3% for laminates 1–6 and 12–15. For these laminates, the bending-twisting coupling, D'_{12}/D'_{66} and D'_{26}/D'_{66} vanishes. The bending-twisting coupling influence factors, see Eq. (1), is a measure of the relative amount of torque, M_{xy} , required to keep the beams from twisting when a bending moment, M_x or M_y , is applied. In the 2D/3D approach, no twist is allowed in the beam analysis step because of the imposed deformation constraints ($\kappa_{xy} = 0$). If the laminate wants to twist under this loading, the current 2D/3D approach will not give accurate predictions. This is illustrated with laminates 7–11, which have non-zero bending-twisting coupling. However, the error in the 2D/3D approach is comparable to the largest of the bending-twisting influence factors D'_{12}/D'_{66} and D'_{26}/D'_{66} . This means that the accuracy of the 2D/3D technique can be assessed a-priori by studying the A'B'D' compliance matrix of the laminate without the need to do any FE analysis. If the bending-twisting influence factors are significant, the torque required to keep the beams from twisting can be calculated from Eq. (1) given the imposed deformation constraints. The calculated torque can then be applied along the edges of the plate (Fig. 10C) in addition to the calculated moments M_x and M_y to get more accurate results. For laminates with unusual lay-ups, there is the possibility that in-plane forces are required to fulfill the constraints imposed. For a beam in the x -direction, the constraints are: $\varepsilon_y = 0$, $\kappa_y = 0$, and $\kappa_{xy} = 0$. This

could potentially lead to in-plane forces N_x and N_{xy} in addition to a torque M_{xy} (see Eq. (1) and Fig. 9). If necessary, these in-plane forces can be treated in the same way as the torque M_{xy} described above.

Table 3 shows that the 2D/3D technique works less well for laminates with multiple plies in the same orientation stacked on top of each other. However, these lay-ups are not common in practice as they increase the risk of delamination and premature failure. The laminates in Table 3 are also relatively thin and contain few repeat units. Table 4 shows the bending-twisting influence factors for symmetric angle laminates [45/−45]_{nS} and quasi-isotropic laminates [0/45/−45/90]_{nS} as the number of repeat units increases. When the thickness reaches 64 plies, the bending-twisting influence factors are less than 2% for both lay-ups, making the developed technique useful for many practical situations.

A flat plate represents the worst case in terms of coupling of deformations between perpendicular cross-sections. If the laminate is curved, there will be a geometric stiffening effect that suppresses coupling between perpendicular cross-sections. An example of this is the

Table 4

The effect of the number of repeat units on the bending-twisting coupling influence factors

Laminate #	Lay-up	Bending-twisting coupling D'_{16}/D'_{66} (%)	Bending-twisting coupling D'_{26}/D'_{66} (%)
16	[45/−45] _{16S}	2.0	2.0
17	[45/−45] _{8S}	4.1	4.1
18	[0/45/−45/90] _{8S}	0.9	1.1
19	[0/45/−45/90] _{4S}	1.6	2.6

rib in case study I. The spring-in of the flanges along the length of the rib will in this case have very little effect on deformations perpendicular to this axis because of the geometric stiffness in this direction.

In this validation study there was no spatial variation in loading or laminate geometry and one cross-section in each direction was sufficient for the analysis. In the general case, where there are gradients in loading and/or laminate geometry, several cross-sections along each coordinate should be taken, as will be illustrated in case study II.

3.4. Case study II: The 777 Aft Strut Trailing Edge Fairing

The Boeing 777 Aft Strut Trailing Edge Fairing is a honeycomb structure with carbon/epoxy skins (Hexcel F593 style 3K-70-PW fabric prepreg) and with film adhesive (CytecFiberite Metalbond 1515) between the prepreg and the over-expanded Nomex honeycomb core (3/16 cell, grade 4) [22]. The fairing is approximately 1.8 m long, 0.3 m high and wide, and is processed on a concave tool (Fig. 11). The fairing is attached to the lower wing skin at four locations along the upper flange and to the Aft Strut Fairing via fasteners at the forward (wide) end joggle. Manufacturing experience has shown that the process-induced deformation of this structure is significant and that the process tool needs to be compensated for the deformation to avoid problems in assembly. To determine the process-induced deformation and the appropriate tool compensation, a total of six parts were measured using a Romer portable coordinate measurement machine (CMM) to determine the tool profile and the matching tool-side part profile at the upper flange locations. The difference between the two data sets gives the total process-induced deformation at each location, which can be compared to model predictions. The process-induced deformations were determined using the presented 2D/3D technique.

Step 1. Select appropriate 2D sections of the 3D structure. Four cross-sections, perpendicular to the

longitudinal axis of the fairing were chosen as measurements revealed that the primary deformation was in these planes, see Fig. 11A. Deformations perpendicular to these planes are small because of the stiffness of the fairing in this direction.

Step 2. Create and run 2D process models of the selected sections. One FE model was created for each section. Each model consists of a FE mesh, initial and boundary conditions, material properties, and cure cycle. The FE meshes were created using the PATRAN pre-processor, based on a CAD description of the geometry of the part. The rest of the model was set-up in the COMPRO process simulation software. The FE mesh created for Section 2 is shown in Fig. 11B. Only one half of the part and tool is modeled due to symmetry.

Step 3. Study and verify the predicted deformations of 2D models. After the models were executed in COMPRO (approximately 1 hour run time on a Pentium III 450 MHz PC), the deformed shapes of the 2D process models were analyzed. All four models showed that the principal mode of deformation is “spring-in” of the flanges (Fig. 13), driven by material anisotropy and the curvature of the fairing. In the present case we are focusing on spring-in at the end of the flanges where the fasteners are located.

Step 4. Create 3D model of the part. Using the FE package ABAQUS version 5.8, a full 3D elastic model of the part was created. The tooling was not modeled, and shell elements were used in a linear elastic analysis, see Fig. 12. The purpose of the 3D model is to study how the deformations of the individual sections interact when the part is fully cured, cooled down, and removed from the process tooling.

Step 5. Isolate cross-sections in the 3D model and match deformations. Strips of the 3D model corresponding to the 2D sections created under Step 1 were isolated, see Fig. 13. The moments that need to be applied to the strip models so that the deformations agree with the 2D process models were determined using the principle of superposition: $\delta_1 = C_{11}M_1 + C_{12}M_2$; $\delta_2 = C_{21}M_1 + C_{22}M_2$, where δ_1 and δ_2 are the displacements from the 2D model, C_{ij} the compliance of the 3D strip model, and M_1 and M_2 the unknown moments required to force the 3D strip model to have the same deformation as the 2D process model.

Step 6. 3D-interaction analysis. The loads determined in the previous step were then applied to the full 3D model shown in Fig. 12. The loads were applied as line loads, varying linearly between the isolated cross-sections, see Fig. 14.

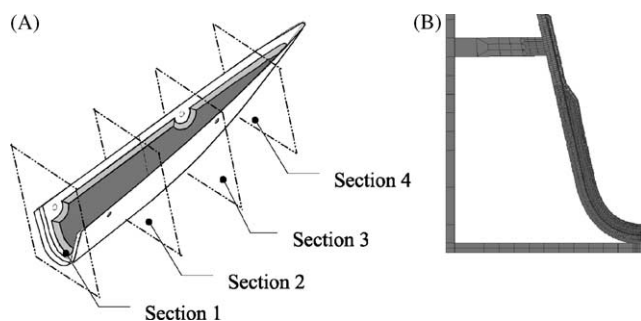


Fig. 11. (A) Boeing 777 Aft Strut Trailing Edge Fairing with four select 2D sections; (B) FE mesh of one half of Section 2, including process tooling.

3.5. Results

Measurements and model results show that the process-induced deformation of primary interest in

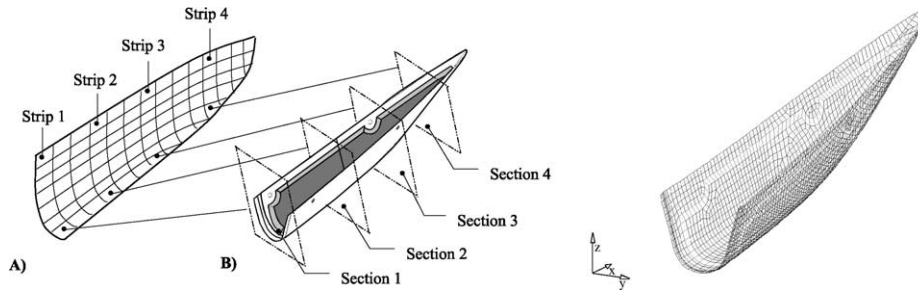


Fig. 12. (A), (B) Schematic of the half 3D FE model showing ‘strips’ corresponding to the four sections used for the 2D COMPRO models; (C) FE mesh of the full 3D model.

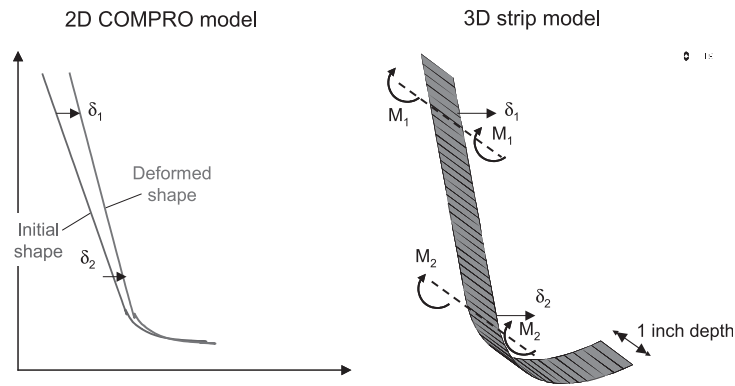


Fig. 13. Schematic of the procedure of matching of displacements between 2D COMPRO model and corresponding 3D strip model.

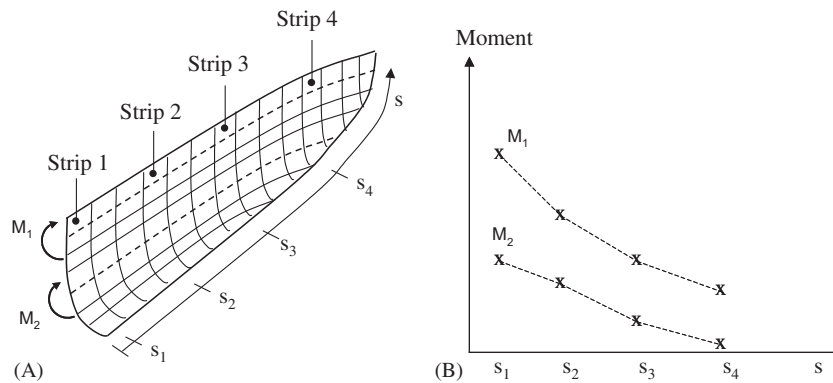


Fig. 14. (A) Schematic of 3D FE model showing the lines on which the moments are applied; (B) schematic showing the linear interpolation of the applied moments per unit width between the four strips.

assembly is spring-in of the flanges, and in particular the resulting gap at the fastener locations at the end of the flanges. Measurements of the gap for six fairings showed consistently that the flanges sprung-in, with a maximum spring-in at the wide end. Fig. 15 shows the average measured gap at the end of the flanges. Error bars represent \pm one standard deviation. The decrease in the total gap towards the tip of the fairing is expected due to the reduction in flange length, and the small decrease in the measured gap between approximately 125 and 375 mm from the wide end is at a location where the

honeycomb core is slightly thicker. Fig. 15 also shows the COMPRO 2D predictions, which are the predictions of free spring-in for the four individual sections removed from the surrounding structure. The agreement between the 2D predictions and measurements is good at Sections 2 and 3, but poor at Section 1. At Section 4 there is no experimental data to compare the predictions against.

The 2D prediction for the total gap at Section 1 is 15 mm. Section 1 is a solid laminate section, and the spring-in is believed to be much greater than the surrounding

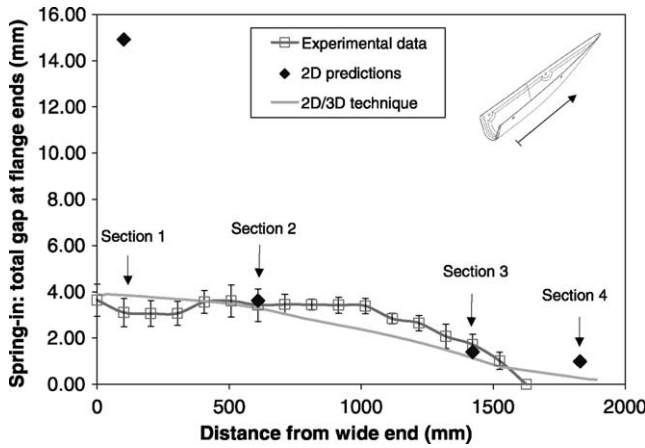


Fig. 15. Comparison of experimental spring-in measurements (both flanges) and model predictions.

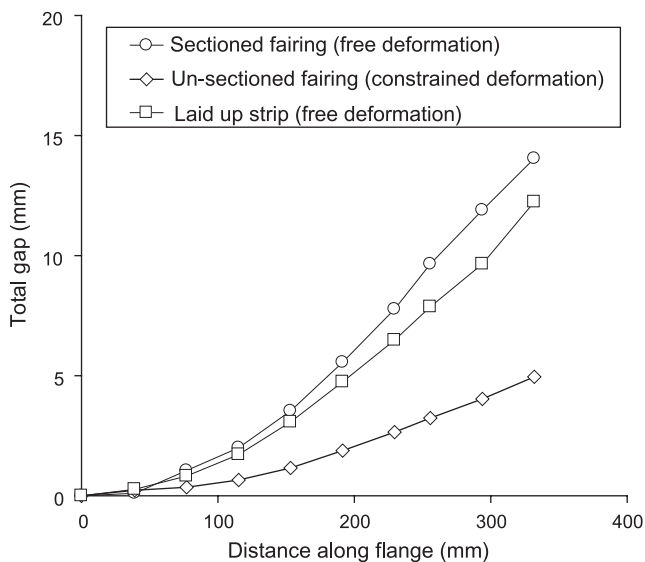


Fig. 16. Measured total gap as a function of the distance along the flange, measured from the centre of the fairing for a sectioned fairing, and un-sectioned fairing, and a lay-ed up strip. All data corresponds to Section 1.

honeycomb structure when removed as a free-body. To verify this, Section 1 was cut off from one of the manufactured fairings and the deformations re-measured (Fig. 16). To further verify the hypothesis that sections behave independently from each other during processing, a 50 mm wide strip of the fairing corresponding to cross-section 1 was laid up and processed independently and the resulting deformations measured, see Fig. 16. From the figure it is seen that the laid up strip behaves similarly to the sectioned fairing, which both have significantly more deformation than the un-sectioned fairing. Note that the sectioned fairing has a total gap of approximately 15 mm, similar to the predictions from the 2D process model at Section 1 (Fig. 15). The constraint of the surrounding structure on Section 1 can be

seen in Fig. 15 (2D/3D technique). When all four sections are connected in a 3D model the free spring-in of the solid laminate section is significantly reduced and the overall agreement between predictions and measurements is reasonably good. Some of the discrepancy between experimental data and the “2D/3D technique” predictions shown in Fig. 15 can be explained by simplifications done in the 3D model due to the geometric complexity of the actual part.

4. Discussion

Although the developed 2D/3D technique gave good results in the current study, it requires engineering judgment and is more prone to error than a one-step FE analysis. The reason a full 3D process analysis is not used is model size. For example, to accurately capture the interaction between the core and the skins in the 777 Aft Strut Trailing Edge Fairing, at least one FE is required in the thickness direction of the adhesive layer. With an adhesive layer thickness of the order of 10^{-4} m, a maximum aspect (length to thickness) ratio of the FEs of 10, and an overall adhesive layer area of approximately 1 m^2 , 10^6 FEs are required to model the adhesive layer alone. The FE model is then solved incrementally in small time steps, making it very time consuming to solve. In contrast, the FE models used for the 2D/3D analysis are readily solved using a basic PC. 3D process modeling is clearly the future but requires an “intelligent” implementation so that large computational effort is used only where it is needed. Work is underway in developing “intelligent” 3D process models.

5. Conclusions

This paper showed that FE based 2D process models in conjunction with simple 3D elastic shell models give good predictions of process-induced deformation of complex-shaped autoclaved composite shell structures. The developed 2D/3D technique is substantially less computationally demanding than a full 3D process model yet retains much of the accuracy of the predictions. A numerical study on flat plates showed that the technique is directly applicable to a wide range of common laminates. Furthermore, the method can be modified and used even when there is a significant bending-twisting coupling in the laminates and in cases with unusual lay-ups.

Acknowledgements

This work is the one of the outcomes of the “Processing for Dimensional Control” project (US Air Force

contract #: F33615-97-C-5006). We thank The United States Air Force Research Laboratory, Materials and Manufacturing Technology Directorate, Wright Patterson Air Force Base, Ohio, USA, for the funding and our contract manager Roger Gerzeski for his effort in leading and coordinating the research. We also would like to thank The Natural Sciences and Engineering Research Council of Canada for providing supplementary funding for the work.

References

- [1] Ridgard C. Accuracy and distortion of composite parts and tools: causes and solutions. In: Tooling for Composites '93, Pasadena, California, 18–19 January 1992: EM93-113.
- [2] Twigg G, Fernlund G, Poursartip A. Measurement of tool-part interfacial stress during the processing of composite laminates. In: 16th ASC Technical Conference, Blacksburg, VA, 9–12 September 2001.
- [3] Rennick TS, Radford DW. Components of manufacturing distortion in carbon fibre/epoxy angle brackets. In: 28th International SAMPE Technical Conference, 4–7 November 1996:189–97.
- [4] Stephan A, Schwinge E, Müller J, Öry H. On the springback effect of CFRP stringers: an experimental, analytical, and numerical analysis. In: 28th International SAMPE Technical Conference, 4–7 November 1996:245–54.
- [5] Nelson RH, Cairns DS. Prediction of dimensional changes in composite laminates during cure. In: 34th International SAMPE Symposium, 8–11 May 1989:2397–410.
- [6] Huang CK, Yang SY. Warping in advanced composite tools with varying angles and radii. *Compos Part A* 1997;28A:891–3.
- [7] Loos AC, Springer GS. Curing of epoxy matrix composites. *J Compos Mater* 1983;17(2):135–69.
- [8] White SR, Hahn HT. Mechanical property and residual stress development during cure of a graphite/BMI composite. *Polymer Eng Sci* 1990;30(22):1465–73.
- [9] Bogetti TA, Gillespie Jr JW. Two-dimensional cure simulation of thick thermosetting composites. *J Compos Mater* 1990;25(3):239–73.
- [10] Bogetti TA, Gillespie Jr JW. Process-induced stress and deformation in thick-section thermoset composite laminates. *J Compos Mater* 1992;26(5):626–60.
- [11] Harper BD, Weitsman Y. On the effects of environmental conditioning on residual stresses in composite laminates. *Int J Solids Struct* 1985;21:907.
- [12] Stango RJ, Wang SS. Process-induced thermal stress in advanced fibre-reinforced composite laminates. *J Eng Industry* 1984;106(1):48–54.
- [13] White SR, Kim YK. Viscoelastic analysis of processing-induced residual stresses in thick composite laminates. *Mech Compos Mater Struct* 1997;4:361–87.
- [14] White SR, Kim YK. Process-induced stress analysis of AS4/3501-6 composite material. *Mech Compos Mater Struct* 1998;5(2):153–86.
- [15] Chen PC, Ramkumar RL. RAMPC-An integrated three-dimensional design tool for processing composites. In: 33rd International SAMPE Symposium, 7–10 March 1988:1697–708.
- [16] Hubert P, Vaziri R, Poursartip A. A two dimensional flow model for the process simulation of complex shape composite laminates. *Int J Numer Meth Eng* 1999;44(1):1–26.
- [17] Johnston A, Vaziri R, Poursartip A. A plane strain model for process-induced deformation of composite structures. *J Compos Mater* 2001;35(16):1435–69.
- [18] Johnston A, Hubert P, Fernlund G, Vaziri R, Poursartip A. Process modelling of composite structures employing a virtual autoclave concept. *J Sci Eng Compos Mater* 1996;5(3-4):235–52.
- [19] Fernlund G, Abdel-Rahman N, Courdji R, Poursartip A, Willden K, Nelson K. Experimental and numerical study of the effect of cure cycle, tool surface, geometry, and lay-up on the dimensional fidelity of autoclave-processed composite parts. *Compos Part A: Manuf* 2002;13(3):341–51.
- [20] Fernlund G, Griffith J, Courdji R, Poursartip A. Experimental and numerical study of the effect of caul-sheets on corner thinning during autoclave processing of composite laminates. *Compos Part A: Manuf* 2002;13(3):411–26.
- [21] Fernlund G, Poursartip A, Nelson K. Modelling of process induced deformations of composite shell structures. In: 45th International SAMPE Symposium and Exhibition, Long Beach, California, 21–25 May 2000, pp. 169–78.
- [22] Fernlund G, Courdji R, Poursartip A, Hendrickson L, Nelson K, George P. Process induced deformations of the Boeing 777 Trailing Edge Aft Strut Fairing. In: 33rd International SAMPE Technical Conference, Seattle, 4–8 November 2001.
- [23] Gibson RF. Principles of composite materials mechanics. McGraw Hill; 1994.
- [24] Callister WD. Materials science and engineering and introduction. 4th ed., 1997, p. 774–800.